PCCP

Accepted Manuscript

ROYAL SOCIETY OF CHEMISTRY

www.rsc.org/pccp

Journal Name

COMMUNICATION

pH-Sensitive fluorophores from locked GFP chromophores by a non-alternant analogue of the photochemical *meta* effect

Received 00th January 20xx,
Accepted 00th January 20xx

DOI: 10.1039/x0xx00000x

www.rsc.org/

Seth Olsen,[a,¶,*] Mikhail S. Baranov[b,c,¶], Nadezhda S. Baleeva,[b,c] Maria M. Antonova,[b] Kenneth A. Johnson,[d] and Kyril M. Solntsev[e,f,*]

We report the synthesis and characterization of a pH-sensitive fluorescence switch based on a conformationally-locked green fluorescent protein (GFP) chromophore. The chromophore differs from fluoroboryl-locked parent by the addition of a titratable alcohol group on the imidazolinone ring. The chromophore is fluorescent at pH ≤ 5, but becomes non-fluorescent at higher pH, where the substituent is ionized. We use a quantum chemical model to show that the mechanism of the fluorescence turn-off is electronically analogous to photochemical *meta* effects in aryl-containing systems.

1. Introduction

The chromophore of the green fluroescent protein (GFP) is a theme from which a great fugue of fluorescence imaging probes has been synthesized.[1] The basic GFP chromophore motif is a *p*-hydroxybenzylidene-imidazolinone species (*p*OH-BDI, cf. **I**, Figure 1). In GFP, this form exists in equilbrium with its conjugate base *p*O$^-$-BDI (**II**). Following excitation of *p*O$^-$-BDI, ESPT (excited-state proton transfer) proceeds to generate the excited state of the phenolate conjugate base (*p*O$^-$-BDI, cf. **II**,**II**$^+$, Figure 1), from which the characteristic strong green fluorescence is observed.[2-5]

For synthetic chromophore models such as *p*OH-BDI in solution, the pKa for the phenol titration site is 8.5.[6] However, neither fluorescence nor ESPT reaction is observed due to competing internal conversion via ultrafast bridge photoisomerization pathways[7], which also effectively quench the fluroescence.[8] ESPT and fluorescence emission are observed in "conformationally locked" derivatives, where

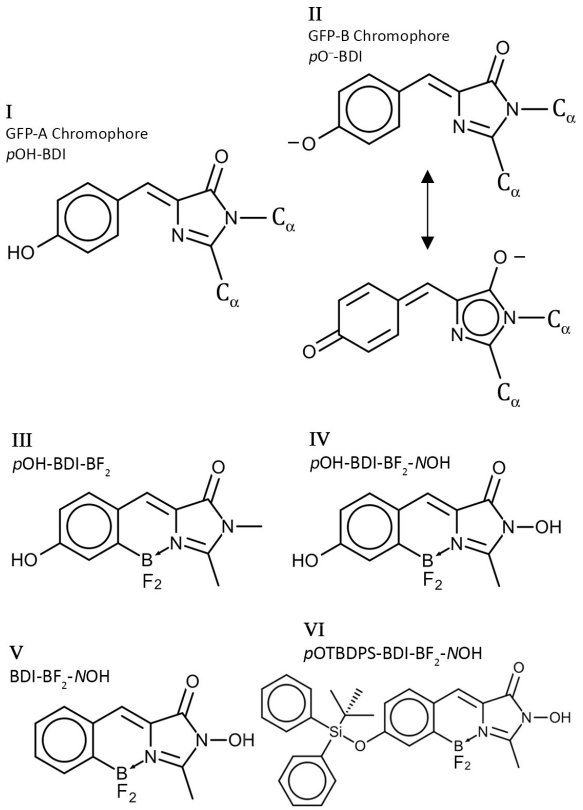

Figure 1. Chromophores based on the BDI motif. "**C_α**" indicates connection to the peptide chain (for protein chromophores) or a methyl group (for synthetic models). Arrow notation is used to represent the coordinate (dative) N-B bond.

[a] School of Mathematics and Physics, The University of Queensland, Brisbane, QLD 4072, Australia. E-mail seth.olsen@uq.edu.au
[b] Institute of Bioorganic Chemistry, Russian Academy of Sciences, Miklukho-Maklaya 16/10, 117997 Moscow, Russia.
[c] Pirogov Russian National Research Medical University, Ostrovitianov 1, Moscow 117997, Russia.
[d] Institute for Cellular and Molecular Biology, The University of Texas at Austin, TX 78712, USA.
[e] Olis Inc, 130 Conway Drive, Bogart, GA 30622, USA.
[f] School of Chemistry and Biochemistry, Georgia Institute of Technology, 901 Atlantic Drive, Atlanta, GA 30332–0400, USA. E-mail solntsev@gatech.edu
¶ Contributed equally

Electronic Supplementary Information (ESI) available: Technical details of quantum chemistry calculations, description of syntheses, additional spectroscopic data, and description of spectral deconvolution method and results. See DOI: 10.1039/x0xx00000x

twisting is hindered by a tethering group such as the difluoroboryl group in *p*OH-BDI-BF_2 (**III** in Figure 1). In *p*OH-BDI-BF_2, photoexcitation leads to ESPT on a 1-3 ns timescale[2]. Strong emission can be observed from both excited states of the photoacid and the product base *p*O^--BDI-BF_2.

In this paper we report synthesis, spectroscopic characterization and theoretical analysis of new derivatives of the fluoroboryl-locked chromophore *p*OH-BDI-BF_2 with a pH-dependent fluorescence turn-off behaviour. The newly reported fluorophore *p*OH-BDI-BF_2-NOH (**IV**, Figure 1) differs from the parent *p*OH-BDI-BF_2 by substitution with an alcohol group at the N position on the imidazolinone ring. We show that the fluorescence of *p*OH-BDI-BF_2-NOH is observable at pH values where the NOH is protonated, but turns off at values appropriate for formation of the NO^- base. We argue on the basis of a theoretical model that the fluorescence turn-off upon NOH deprotonation is electronically analogous to the photochemical *meta*-effect in chromophores containing an aryl ring with mesomeric electrodonating substitutents placed *meta* to the conjugated chromophore chain[8-15].

2. Results

2.1 *Synthesis of chromophores*

The chromophores *p*OH-BDI-BF_2-NOH (**IV** in Figure 1 and Scheme 1), *p*H-BDI-BF_2-NOH (**V**) and *p*OTBDPS-BDI-BF_2-NOH (**VI**) were synthesized. The molecule *p*OH-BDI-BF_2-NOH (**IV**) is the new fluorescence switch; BDI-BF2-NOH (**V**) and *p*OTBDPS-BDI-BF_2-NOH (**VI**) were also synthesized for use as references for comparison. The former, **V**, has an unsubstituted aryl ring. The syntheses are presented on Scheme 1. Conformationally locked chromophore analogs (**IV-VI**) were synthesized from non-locked imidazolones **3** using boron tribromide and molecular sieves via a recently reported borylation reaction.[16-17] The synthetically labile OH group was initially protected using a TBDPS group, while the initial N-hydroxy imidazolones **2** were synthesized using the typical approach from the corresponding oxazolones **1**.[16, 18] Details and analytical chemistry data are presented at the end.

2.2 *Optical properties*

Spectroscopic parameters for the main absorbance and emission bands of the NOH acids *p*OH-BDI-BF_2-NOH, BDI-BF_2-NOH (**V**, Figure 1), and *p*OTBDPS-BDI-BF_2-NOH (**VI**, Figure1) are listed in Table 1 in different solvents in the presence of 1 mM trifluoroacetic acid (TFA). The TFA was used to ensure protonation of the NOH. The absorbance and emission of *p*OH-BDI-BF_2-NOH are similar to those reported for the parent locked chromophore *p*OH-BDI-BF2[16]. The spectral characteristics of *p*OTBDPS-BDI-BF_2-NOH are similar to of *p*OH-BDI-BF_2-NOH but with slightly blue-shifted absorbance and emission. The emission shift is larger in MeOH than in the non-protic solvents. The solvatochromism appears to be weak, as observed in other neutral GFP chromophore models[6].

There is an order-of-magnitude loss of fluorescence

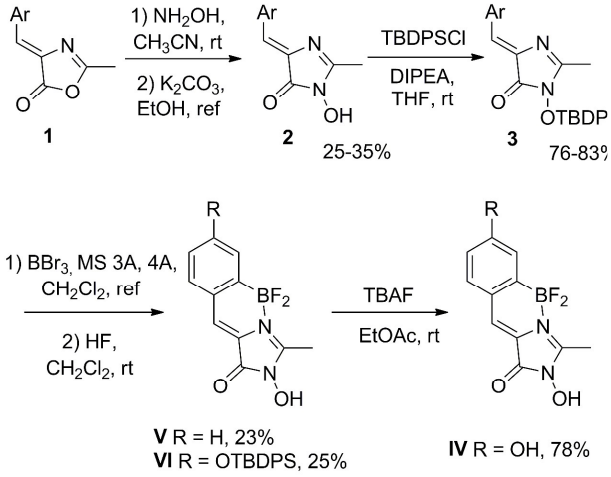

Scheme 1. Synthesis of chromophores *p*OH-BDI-BF_2-NOH (**IV**), BDI-BF_2-NOH (**V**) and *p*OTBDPS-BDI-BF_2-NOH (**VI**).

Table 1. Absorbance and emission maxima (nm) and fluorescence quantum yield measurements for *p*OH-BDI-BF_2-NOH (**V**), BDI-BF_2-NOH (**VI**) and *p*OTBDPS-BDI-BF_2-NOH (**VII**). Measurements were made in the presence of 1 mM trifluoroacetic acid in the solvents indicated.

Solvent	*p*OH-BDI-BF_2-NOH (**IV**)			*p*H-BDI-BF_2-NOH (**V**)			*p*OTBDPS-BDI-BF_2-NOH (**VI**)		
	QY	ABS	EM	QY	ABS	EM	QY	ABS	EM
H_2O	0.12	412	485	NA	NA	NA	NA	NA	NA
MeOH	0.20	417	479	0.02	371	447	0.04	407	457
CH_3CN	0.64	407	466	0.01	365	428	0.43	403	461
DMSO	0.05	419	482	NA	NA	NA	0.03	407	463
Dioxane	0.68	418	462	0.03	368	406	0.28	414	457
Hexane	NA	NA	NA	0.03	370	395	0.52	421	460

quantum yield going from *p*OH-BDI-BF_2-NOH to *p*OTBDPS-BDI-BF_2-NOH and BDI-BF_2-NOH. The quantum yield in any solvent for which data on all species is available decreases in the order *p*OH-BDI-BF_2-*N*OH, *p*OTBDPS-BDI-BF_2-*N*OH, BDI-BF_2-NOH. Overall, the data suggest that the solvent basicity and polarity quenches the emission more efficiently than the solvent proticity/acidity (in the Kamlet-Taft sense)[19,20]. Details of regression of the QY against the solvent Kamlet-Taft parameters are in the Supplement.

Figure 2 shows absorbance spectra of *p*OH-BDI-BF_2-NOH and *p*OTBDPS-BDI-BF_2-NOH in 50 mM phosphate buffer at different pH. For each species, there is a change in the spectrum visible at pH near 4-5, visible as a slight blue shift of the peak and the development of a broader red tail. The top right inset of Figure 2 shows this by plotting the absorbance near 438 nm, which shows the increase in absorbance in this region near pH 5. The changes near pH 5 will be assigned to deprotonation of the *N*OH group. For *p*OH-BDI-BF_2-NOH, there is a further significant change near pH 8-9, visible as the development of an intense red-shifted absorbance. An isosbestic point near 435 nm is apparent. The spectral changes in the absorbance spectrum of *p*OH-BDI-BF_2-NOH near pH 8 are assigned to subsequent titration of the phenol to form the dianion pO^--BDI-BF_2-NO^-.

The chromophore *p*OH-BDI-BF_2-NOH is a pH-dependent fluorescence switch, showing visible fluorescence at low pH. Emission data for *p*OH-BDI-BF_2-NOH following photoexcitation near either peak of the absorbance spectrum (390 nm and 435 nm) are shown in Figure 6. Above pH ~ 5, the fluorescence is quenched.

From spectrophotometric titration of absorbance and emission, we were able to obtain estimates of ground-state pK_a and excited-state pK_a^* values for the NOH and phenolic

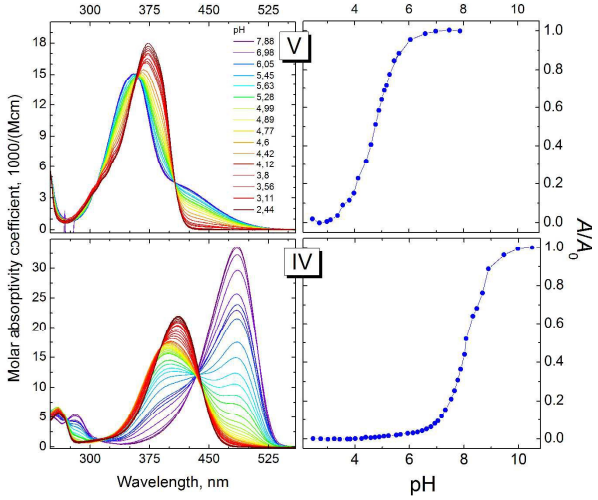

Figure 2 *Top row.* Absorbance spectra of BDI-BF_2-*N*OH (**V** in Figure 1) in 50 mM phosphate buffer at different pH. Relative absorbance at 438nm is shown to right. *Bottom row.* Absorbance spectra of *p*OH-BDI-BF_2-*N*OH (cf. Figure 1, **IV**) in 50 mM phosphate buffer at at different pH. Relative absorbance at 490 nm is shown to right.

titration sites using an SVD-based deconvolution treatment

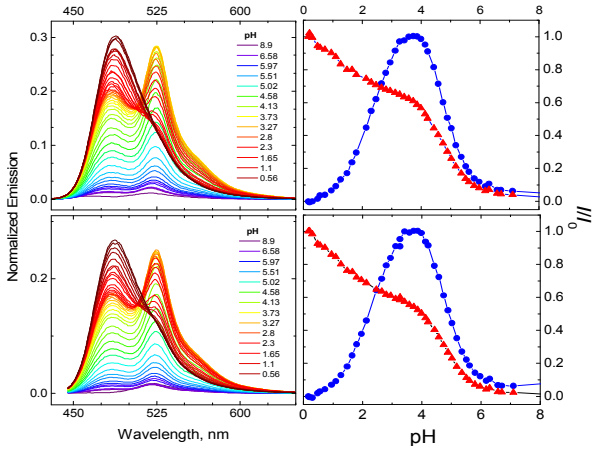

Figure 3 *(Left column)* Emission spectra of *p*OH-BDI-BF_2-*N*OH (**IV** in Figure 1) in 50 mM phosphate buffer excited at 390 nm *(top)* and 435 nm *(bottom). (Right column)* Normalized relative emission intensity measured at 525 nm *(blue dots)* and at 485 nm *(red triangles)*.

(using KinTek Explorer software, www.kintekcorp.com). This yielded a set of 3 ground p*K*a's and excited state p*K*a*'s. These are listed in Table 2. Ground state pK_a's near 5 and excited-state pK_a^*'s near 4 are assigned to the imidazolinone *N*OH titration site. That these values fall in a narrow range for different *para* substituents suggests that inductive interactions between the *para* group and the NOH site are weak. For *p*OH-BDI-BF_2-*N*OH, a new ground state pK_a ~ 9 is observed, and a new excited state pK_a^* ~ 2, which we assign to the phenoxy site. This confirms that photoacidity of the phenoxy site is retained in the *N*OH-substituted derivative. This pK_a^* value is close to the excited-state phenolic pK_a^* of the parent chromophore *p*OH-BDI-BF_2 reported in an earlier study[16]. A third pK_a^* ~ 0.5 was produced by the deconvolution algorithm, which was required to fit a rise in emission at very low pH (see Supplement). The nature of such fluorescence increase under such low-pH conditions is unclear. A description of the deconvolution is available in the Supplement. We summarize

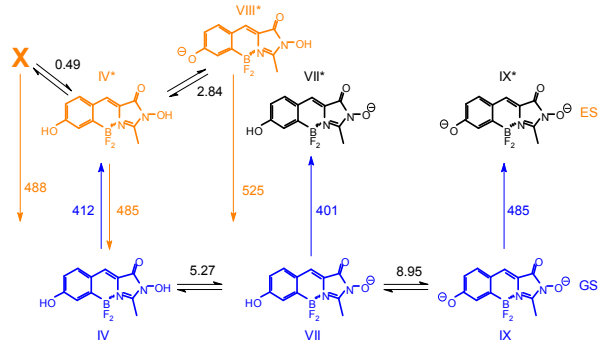

Figure 4. Proposed kinetic scheme for explaining pH-dependent absorbance and emission measurements. GS – ground state, ES – excited state. Blue numbers correspond to absorbance maxima of corresponding species, orange numbers correspond to emission maxima of corresponding species, black numbers are pKa values in GS and ES.

our assignments of the titrating species, as informed by the quantum chemistry and previous studies[16], in Figure 4.

2.3 *Theoretical calculations*

In this section, we describe quantum chemistry calculations that will help to explain the fluorescence turn-off in *p*OH-BDI-BF_2-*N*OH at pH > 5. The quantum chemistry results reported in this paper will be based on state-averaged complete active space self-consistent field (SA-CASSCF) theoretical models[21-22]. In this paper we use the string `SA*X*-CAS(*N*,*M*)` to refer to a *X*-state-averaged SA-CASSCF calculation with *N* electrons distributed over *M* orbitals. With this notation, a two-state, four-electron, three-orbital model (such as applied here and earlier[23-25]) would be referred to as a SA2-CAS(4,3) model. The basis set was the correlation consistent double zeta basis set cc-pvdz described by Dunning[26]. All calculations were performed with the Molpro software[27]. The SA-CASSCF results will be discussed in a Boys(-Rüdenberg)[28] localized orbital representation. The Boys orbitals are the orbitals that maximize the sum of distances between orbital charge centroids. Subotnik and colleagues have contributed an excellent account of the Boys localization, it's history and interpretation[28].

Optimized geometries for a selection of protonation states were obtained by optimization on the ground electronic state calculated using an MP2 model[29] with a cc-pvdz basis set[26]. The decision to notate the NB bond as a dative bond in the Figures was based upon the observation that the NB bond length shortened significantly (by 0.1Å) upon NOH deprotonation, and this deprotonation is also be expected to favor bonding structures with a covalent NB bond.

The absolute energies of the ground states of anions *p*O$^-$-BDI-BF_2-NOH (**VIII**, Figure 6) and *p*OH-BDI-BF_2-NO$^-$ (**VII**, Figure 6), both of which are conjugate to *p*OH-BDI-BF_2-NOH, may be compared directly, since the atomic constituency (thus, electron number and nuclear charge) are the same. The ground state energy of *p*O$^-$-BDI-BF_2-NOH was found without any solvent model to be 2.8 kcal/mol lower than the ground state energy of *p*OH-BDI-BF_2-NO$^-$. We would intuitively predict better solvation of the *p*OH-BDI-BF_2-NO$^-$ base than the phenolate, because in the latter case the negative charge can delocalize by conjugation to the oxonol chain (cf. **II**,**II**$^+$ in Figure 1), whereas in the former case it cannot, leading to more localized charge and better polar solvation. The point is that the two are close enough that neither could be ruled out of the ground or excited-state chemistry, and we expect that the balance could depend sensitively on the solvation model.

We attempted to obtain for the molecules *p*OH-BDI-BF_2-NOH , *p*OH-BDI-BF_2-NO$^-$ and *p*O$^-$-BDI-BF_2-NOH a solution to the 2-state averaged, 4-electron-in-3-orbital SA-CASSCF[21] (SA2-CAS(4,3)) problem, such as described for other BDI models[23-25, 30]. Many BDIs and derivatives have similar solutions to this problem, as has been described in previous work[23-25, 30-32]. In these cases, the solution found maps the electronic structure of BDI onto an allylic system, which can be identified with the bridge. The importance of the analogy to allyl has been emphasized also by Bravaya, Krylov and coworkers, using a distinct theoretical approach.[33] The solution has been proposed as a model of the low-energy oxonol electronic subsystem.[23] A similar SA-CASSCF can also be found for a variety of monomethine cyanines.[34] It's ubiquity reflects the

Table 2. Ground state-pK_a's and excited-state pK_a*'s obtained from deconvolution of spectrophotometric absorbance and emission titration data for **IV**, **V** and **VI** in water-methanol solution. Emission data was only available for **V**, in which case the values without parentheses correspond to excitation at 390 nm; those with parentheses to excitation at 435 nm.

Low pH Species	pK_a	pK_a*'s
*p*OH-BDI-BF_2-NOH	8.95±0.03, 5.27±0.02	4.87±0.03, 2.84±0.08, 0.49±0.13 (4.92±0.03, 2.83±0.08, 0.49±0.10)
BDI-BF_2-NOH	5.42±0.02	NA
*p*OTBDPS-BDI-BF_2-NOH	5.24±0.02	NA

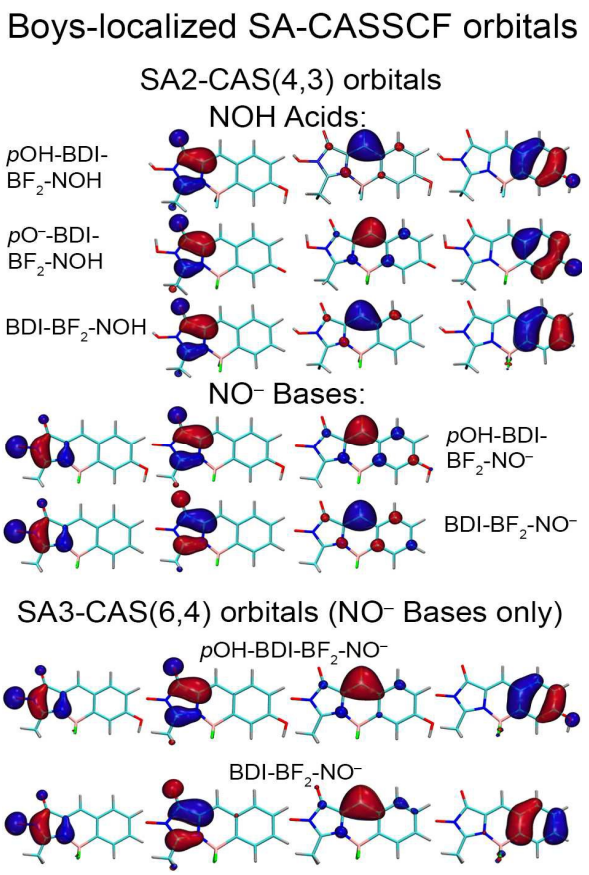

Figure 5 Boys-localized SA-CASSCF solutions for *p*OH-BDI-BF_2-NOH, BDI-BF_2-NOH and their monoanionic conjugate bases. *Top 3 rows:* Converged SA2-CAS(4,3) active spaces for NOH acids (from top down) *p*OH-BDI-BF_2-NOH, *p*O$^-$-BDI-BF_2-NOH and BDI-BF_2-NOH. There are active orbitals localized on the aryl, bridge and imidazolinone groups; this structure has been reported for SA2-CAS(4,3) solutions of many BDI derivatives. *Middle 3 rows:* SA2-CAS(4,3) active spaces for NO$^-$ bases *p*OH-BDI-BF_2-NO$^-$ and BDI-BF_2-NO$^-$. In these cases, the SA-CASSCF converges to a distinct structure where the aryl orbital (far right above) is missing, replaced by a second imidazolinone orbital (far left). The new imidazolinone orbital has weak amplitude on the bridge-adjoining carbon. *Bottom 2 rows:* SA3-CAS(6,4) active space orbitals for the same NO$^-$ bases. The orbital space is seen to span the *union* of the SA2-CAS(4,3) active spaces for the NO$^-$ base and the corresponding NOH acid. The two excited states emerging from the SA3-CAS(6,4) calculation have the structure of the SA2-CAS(4,3) excited states for the acid and the base, with the lower electronic state corresponding to the SA2-CAS(4,3) excited state of the base.

dominance of the charge-resonance in the low-energy electronic structure of these systems[34]. The SA2-CAS(4,3) model reproduces, at least semi-quantitatively, results for BDI derivatives that have been obtained with larger active spaces or other non-CASSCF benchmark calculations[35-38]. For monomethine cyanines, which have a similar solution to the SA2-CAS(4,3) problem, the solution has been shown to correspond to a "Pauling point", which describes a full π-electron CASSCF better than intermediate active spaces[34].

The converged active spaces we obtained are shown in Figure 5. A key result of this section is that the previously described CAS(4,3) solution characteristic of BDI's with a bright S_1 excited state, could not be obtained for the NO^- bases. Instead, the SA2-CAS(4,3) procedure converged to a distinct set of active space orbitals for *p*OH-BDI-BF_2-NO^-, heralding a qualitatively different chemistry of the excited state. A similar solution was also found for BDI-BF_2-NO^-, suggesting that this is a general behavior of similar monoanionic NO^- derivatives.

We provide cartesian coordinates of geometries, SA-CASSCF state energies, state-averaged natural orbital graphics and corresponding occupation numbers in the Supplement. These data can help the reader to identify the appropriate solutions, should she attempt to reproduce the results.

The failure to obtain the previously characterized SA2-CAS(4,3) solution for *p*OH-BDI-BF_2-NO^- and BDI-BF_2-NO^- is a result, because that solution has been observed to occur in so many other cases.[23-24, 30-32, 34, 39] We interpret the failure to obtain a similar solution for the NO^- bases as a herald of qualitatively different low-energy electronic structure of the lowest excited state.

For the NO^- bases, we found that the solution to the SA2-CAS(4,3) problem had a qualitatively different structure to the corresponding acids. For the bases, the active space at convergence had the phenoxy orbital replaced by a second imidazolone orbital with a node on the bridge-adjoining atom. These solutions are illustrated in the middle rows of Figure 6.

Electronic excitation energies and dipole observables associated with the $S_0 \rightarrow S_1$ transition described by the SA2-CAS(4,3) solutions for *p*OH-BDI-BF_2-NOH, and its conjugate bases *p*OH-BDI-BF_2-NO^- and *p*O^--BDI-BF_2-NOH are collected in Table 3. A internally contracted multi-reference second-order Schrödinger perturbation theory correction[40] was applied to the excitation energies of the SA2-CAS(4,3) reference states, with only core excitations excluded. The agreement between calculated electronic gaps and measured absorbance bands in Table 1 is providential. Better agreement could not have been expected, given the compact active space model used and the lack of a solvation model in the calculations. For both cases, the calculated value is ≤ 0.1 eV removed from the relevant peak absorbance energy, which is better than the expected accuracy of the methods used according to relevant benchmarks[41]. This is true of all species with first electronic gaps in the UV/Vis region.

Table 3. Calculated S_1-S_0 excitation energies (ΔE, eV), photon wavelengths (nm), difference dipole moment norm (Δμ, D) transition dipole moment norm (|Δμ|, D) and oscillator strengths (*f*) for some chromophores studied. Energies were calculated with a multi-reference perturbation theory treatment based on the SA-CASSCF solutions in Figures 2 and 3. The SA-CASSCF dipole elements and the perturbed excitation energies were used to calculate the oscillator strengths.

Species	ΔE(eV) /λ (nm)	Δμ(D)	$\|\mu_{12}\|$(D)	*f*
*p*OH-BDI-BF_2-NOH	3.04/408	7.5	7.8	0.70
*p*OH-BDI-BF_2-NO^-	1.01/1228	10.3	2.2	0.02
pO^--BDI-BF_2-NOH	2.68/463	4.0	9.4	0.88
BDI-BF_2-NOH	3.35/370	7.4	7.2	0.65
BDI-BF_2-NO^-	0.94/1319	10.4	2.2	0.02

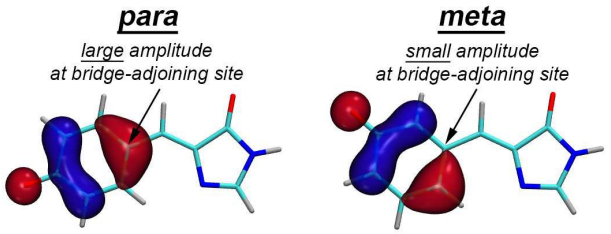

Figure 6 Local frontier orbital structure on the aryl ring of *para*-O^- and *meta*-O^--substituted BDI derivatives .

The results show a significant change in the excited state energy and dipole properties upon titration of the NOH. When the group is protonated, the excitation energy, and difference and transition dipoles are consistent with previous results for GFP chromophore using the same electronic structure model[23-25, 31]. When the NOH group is deprotonated, the transition is much dimmer and red-shifted.

Since we find experimentally that the NOH acids and NO^- bases have similar orders of UV/Vis absorbance intensity, it cannot be the case that the dim S_1 state described in Table 3 is the absorbing state. We verified that the characteristic bright excited state exists in the NO^- bases, by expanding the SA-CASSCF model and for the NO^- bases to a 6-electron-in-4-orbital, 3-state-averaged model (SA3-CAS(6,4)). The converged SA3-CAS(6,4) active space structures are shown in Figure 6, bottom, for *p*OH-BDI-BF_2-*N*O^- and BDI-BF_2-NO^-. As is clearly seen, the active space spans the SA2-CAS(4,3) spaces characteristic of molecules with both dim and bright S_1 states. The SA3-CAS(6,4) spectra had the lowest adiabatic excited state S_1 as the dim trap state and the second excited state S_2 as the bright excited state reported in various studies of BDI derivatives.[23-25] Apparently the bright state exists as S_2 in the electronic spectrum of the NO^- bases, at energies similar to the corresponding acids, but it is no longer the lowest electronic excited state.

Our calculations were performed in the absence of any solvent model. The data in Table 3, showing a larger difference dipole for excitation to the dim state in the NO^- bases, suggest that solvent polarity will widen the gap more than for this excitation than for excitation to the bright state. Polar effects could potentially be described by a polar continuum model, if an appropriate solvent cavity were chosen. However, the data in Table 1 and previous analyses suggest that solvent properties other than polarity are also important, and the

treatment of these effects in quantum chemistry calculations is less developed than for polar solvent effects. We decided to stick with gas-phase calculations and to emphasize qualitative chemical implications.

3. Discussion

We argue that the fluorescence turn-off behavior of *p*OH-BDI-BF_2-NOH at pH ≥ 5 is the manifestation of an effect analogous to the photochemical *meta*-effect observed in chromophores containing aryl ring(s) with strong mesomeric electrodonating groups placed *meta* to the conjugated chromophore chain[8-15]. To justify this explanation, we first quickly review the *meta*-effect for aryl-containing systems.

Meta-Effects The formation of the fluorophore in *para*-OH and *para*-O^- BDIs depends on the conjugation of the O^- donor to the bridge to form the conjugated π-electron chain. This is achievable for a mesomeric donor substituent in the *para* position on the aryl ring, but not the *meta* position.

The behaviour of *meta*-OH and *meta*-O^- BDIs is different from the corresponding *para*- analogues. Following excitation in aqueous solution, *meta*-OH-BDI undergoes ESPT from the phenoxy on a sub-picosecond timescale, yielding an anionic excited state that decays on a longer (sub-ns) timescale[8]. In non-aqueous solutions, no ESPT occurs, and the excited state of the product decays via internal conversion on a sub-ns timescale.[42-43]

Yang and coworkers investigated the behaviour of BDI derivatives with *para*-NH_2 and *meta*-NH_2 groups on the aryl ring[14-15, 44]. These models of interest because NH_2 is a mesomeric electrodonating group intermediate between OH and O^- on the Hammett (σ) and Brown-Okamoto (σ^+) substituent scales[45]. They found that, relative to the *para*-NH_2 model, the *meta*-NH_2 species showed much slower radiative and non-radiative decay times[14-15, 44].

The *meta-para* dichotomy in BDI derivatives is observed in other conjugated π-electron systems. Long-lived, weakly radiating states occur in systems where a sufficiently electron-donating or mesomeric group placed *meta* with respect to the conjugated π-electron chromophore chain. An example is observed in 3- vs. 4-hydroxystilbenes[42-43]. The *meta*- (3-)hydroxystilbenes are photoacidic with a long-lived excited-state product, while the *para*- (4-)hydroxystilbenes undergo ultrafast photoisomerization on a timescale that suppresses the photoacidity[42-43]. In *para*-amino stilbenes, photoisomerization dominates the photobehaviour, while in contrast *meta*-amino analogues show low-intensity red-shifted emission from a long-lived excited state[11]. The singlet lifetime for *meta*-substituted species can extend into the 10-20 ns range[10-11].

The divergent behaviour of *para*- and *meta*-OH/O^- BDIs can be understood in terms of the relevant frontier orbital structure of the aryl ring. This is illustrated in Figure 2, which shows relevant frontier (active) occupied orbitals for a *para*-OH-BDI derivative and its *meta* analogue. When the substituent is *para* with respect to the bridge, the relevant occupied frontier orbital has large amplitude on the bridge-adjoining carbon. This allows easy coupling into the bridge and the remainder of the chromophore system. When the substituent is *meta*, the relevant occupied orbital has very low amplitude at the bridge-adjoining site so coupling is weak. The development of a bright fluorophore requires strong coupling, and so only occurs in the *para* case. In the *meta*- case, the lack of strong coupling instead leads instead to long-lived trap states with low dipole strength (thus long radiative lifetime).

The appropriate hydrocarbon reference for the imidazolinone ring is the cyclopentadienyl anion, which is aromatic and therefore, like aryl, has a degenerate two-dimensional frontier orbital space. As cyclopentadienyl anion is heteroaromatic and non-alternant, classification of sites as *meta*- vs. *para*-like is not straightforward, and the heteroatomic potential will lift the degeneracy at low order. A *meta*-like photochemical effect should be achieveable, though, if the are two frontier ring orbitals distinguished by overlap with the bridge. If the relevant uncoupled orbital can be raised to the frontier by substitution, then electronic excitations uncoupled to the bright conjugated chromophore will become accessible. By appending a titratable OH group on the imidazolinone in a position with "meta-like" behaviour, it may be possible to introduce a low-energy dim state in the spectrum upon titration of the substituent. If the trap state lies lower in the spectrum than the oxonol excited state, Kasha's rule predicts population will flow to the trap state.

The behavior of the SA-CASSCF solutions that we have examined for these molecules shows that NOH deprotonation introduces a new orbital into the imidazolinone frontier, which has large amplitude on the amine *N* site but small amplitude on the bridge-adjoining carbon. The electronic structure of this lowest energy excited state in the base *p*OH-BDI-BF_2-NO^- is dominated by excitations out of this orbital. The corresponding lowest excited state was found to lie at very low energy and to have a dipole strength two orders of magnitude smaller than for the bright state observed and calculated for *p*OH-BDIs. This is the rationale behind our identification of the fluorescence turn-off in *p*OH-BDI-BF_2-NOH with photochemical *meta*-effects in aryl-containing systems.

The molecule *p*OH-BDI-BF_2-NOH shows the strongest fluorescence turn-off behavior of all the molecules listed in Table 1, at least in part because it has the highest fluorescence quantum yield in the protonated state. To explain the experimental fluorescence quantum yield trend for the molecules *p*OH-BDI-BF_2-NOH, BDI-BF_2-NOH, and *p*OTBDPS-BDI-BF_2-NOH under low-pH conditions (cf. Table 1), we postulate that high fluorescence is favored by accessibility of the charge-transfer configuration with charge on the imidazolinone oxygen (cf. resonant configuration for anion in Figure 1). This will occur only for molecules in which the charge-transfer configuration lies low enough to be sufficiently populated in the adiabatic excited state. Groups like TBDPS are electron-withdrawing relative to H[45], and so we expect the OTBDPS to have intermediate electron-withdrawing power between OH and H. This suggests that the charge-transfer diabatic energy gap should increase in the order *p*OH-BDI-BF_2-NOH, *p*OTBDPS-BDI-BF_2-NOH, BDI-BF_2-NOH. We find that the measured fluorescence quantum yields decrease in the same order. The observation that basicity and polarity kill the emission much

more efficiently than the proticity, also provides some support. In polar solvents, an increase in the charge-transfer gap is expected. In protic solvents, the charge-transfer gap may be narrowed by protic coordination of the imidazolinone. The notion that protic coordination of the imidazolinone could stabilize the excited state is supported by a comparison of the gas-phase absorbances of series of *p*OH-BDI models with groups appended that can or cannot accomplish such coordination[46]. It is also supported by theoretical predictions that *para*-OH BDIs protonated at both the phenoxy and imidazoloxy sites should have an electronic gap that is nearly as low as for the anionic form[23, 25].

For the core *p*OH-BDI motif, theoretical discussions tend to highlight bridge photoisomerization as a deactivation mechanism[25, 33, 37-38]. There is some extant experimental evidence contraindicating large-amplitude torsional motion in the quenching mechanism.[7, 14-15, 44, 47-48] The presence of the locking group prevents large-amplitude torsion in the present case. The lowest-energy excited state of the NO^- bases is proposed on the basis of our calculations to be a dim trap state analogous to dim states observed in chromophores with a photochemial *meta*-effect. We calculate the oscillator strength for this transition to be 1-2 orders of magnitude smaller than for transition to the bright excited state. Such an oscillator strength would be consistent with a radiative lifetime on the order of tens of ns, as observed in *meta*-aminostilbenes[11]. We attempted to observe long-wavelength fluorescence from the NO^- bases in the spectral window suggested by the calculations (~1200 nm), but the experiments were complicated by solvent transitions in this region and no emission could be observed. We cannot definitively conclude based on the current work whether the dim low-energy trap state of the NO^- bases decays radiatively or not, or what other possible decay mechanisms may exist for the non-fluorescent state. If it does radiate, then our calculations suggest that the emission should occur outside the visible spectrum, at photon energies below 1 eV.

For the NO^- bases, our calculations indicate that the S_2 state is to be identified with the bright S_1 excited state of the acids and other BDI derivatives[23-25, 30]. The present experimental data are insufficient to say much about the mechanism of internal conversion from S_2 to S_1 in these cases. Our calculations suggest *prima facie* that proton ejection from the NOH, either extramolecular or intramolecular, could concievably be a candidate reaction coordinate. However, a more detailed examination of the excited state potential surfaces, at least, would be needed to provide further support for this mechanism. We did find in preliminary calculations that displacing the proton from the NOH to the neighboring carbonyl was energetically allowed (exothermic) in the excited state. We did not attempt to model the energetics of proton ejection to solvent. A conclusive identification of the reaction coordinate for S_2->S_1 internal conversion requires, on the theory side at least, a broader survey of the relevant excited-state potential energy surfaces.

At pH > 9, both NOH and phenol protons should be dissociated, leading to the dication pO^--BDI-BF_2-NO^- (**IX**, Figure 4). No visible fluorescence was detected in this regime. Calcuations on the dianion indicated that the bright and dim states were highly mixed for this species, but were consistent with our results for the phenolic NOH bases. It is conceivable that excitation into the bright visible absorbance band leads to a dim state like the phenolic NO^- bases, leading to a similar fate, but we are unable to rule out the possibility that a distinct decay mechanism exists for these species at high pH ≥ 9.

4. Experiments

4.1 *Materials and methods*

Commercially available reagents were used without additional purification. For column chromatography, E. Merck Kieselgel 60 was used. NMR spectra were recorded on a 700-MHz Bruker Avance III NMR at 293 K. Chemical shifts are reported relative to residue peaks of $CDCl_3$ (7.27 ppm for ^1H and 77.0 ppm for ^{13}C) or DMSO-d6 (2.51 ppm for ^1H and 39.5 ppm for ^{13}C). Melting points were measured on a SMP 30 apparatus. High-resolution mass spectra were obtained on an Agilent 6224 TOF LC/MS System (Agilent Technologies, Santa Clara, CA, USA) equipped with a dual-nebulizer ESI source. Data acquisition and analysis was performed by the MassHunter Workstation software (Agilent Technologies, Santa Clara, CA, USA).

4.2 *Synthesis*

4.2.1 Synthesis of (Z)-4-arylidene-2-oxazol-5(4H)-ones (1)

(Z)-4-arylidene-2-oxazol-5(4H)-ones **1** were synthesized as reported previously[18].

4.2.2 Synthesis of (Z)-4-arylidene-1-hydroxy-1H-imidazol-5(4H)-ones (2)

To the suspension of corresponding oxazolone (0.05 mole) in CH_3CN (100 mL) hydroxylamine hydrochloride (7.99 g, 0.115 mole) and Et3N (8.4 ml, 0.115 mole) were added upon stirring. The mixture was stirred for 1 h at room temperature and the solvent was removed in vacuum. Potassium carbonate (15.87 g, 0.115 mole), cesium carbonate (3.84 g, 0.0115 mole) and DMF (150 ml) were added and the mixture was refluxed for 5-10 min (observed by TLC – EtOH:$CHCl_3$ 1:10). The mixture was evaporated and dissolved in water (300 mL) and acidified by HCl to pH=5. The mixture was extracted by EtOAc (2x150 mL), washed by water (1x50 mL), brine, dried over anhydrous Na_2SO_4. The solvent was evaporated and the product was purified by column chromatography (EtOH:$CHCl_3$).

(Z)-4-benzylidene-1-hydroxy-2-methyl-1H-imidazol-5(4H)-one.

Yellowish solid, 3.43 g (34%); mp = 205-208°C with decomposition; 1H NMR (700 MHz, DMSO) δ 10.92 (s, 1H), 8.21 (d, J = 7.3 Hz, 2H), 7.46-7.41(m, 3H), 7.03 (s, 1H), 2.32 (s, 3H). 13C NMR (176 MHz, DMSO) δ 165.0, 162.3, 135.7, 133.8, 132.1, 130.2, 128.6, 126.0, 13.7; HRMS (ESI) m/z: 203,0813 found (calcd. for $C_{11}H_{11}N_2O_2$, [M+H]+ 203.0821).

(Z)-1-hydroxy-4-(4-hydroxybenzylidene)-2-methyl-1H-imidazol-5(4H)-one.

Yellow solid, 2.83 g (26%); mp approximately 280°C with decomposition; 1H NMR (700 MHz, DMSO) δ 10.8 (bs, 1H), 10.1 (bs, 1H), 8.07 (d, J = 8.8 Hz, 2H), 6.94 (s, 1H), 6.84 (d, J = 8.8 Hz, 2H), 2.28 (s, 3H); 13C NMR (176 MHz, DMSO) δ 165.0,

159.9, 159.8, 134.4, 133.0, 126.8, 125.1, 115.8, 13.6; HRMS (ESI) m/z: 219.0755 found (calcd. for $C_{11}H_{11}N_2O_3$, [M+H]+ 219.0770).

4.2.3 Synthesis of (Z)-1-((tert-Butyldiphenylsilyl)oxy)-4-arylidene-2-methyl-1H-imidazol-5(4H)-ones (3)

The solution of corresponding N-hydroxy imidazolone (3 mmol), diphenyl(tert-butyl)silyl chloride (4 or 8 mmol), diisopropylethylamine (4.5 or 9 mmol) and imidazole (31 mg, 0.3 mmol) in dry THF (100 mL) was stirred at the room temperature for 48 hours. The mixture was evaporated and 150 mL of $CHCl_3$ was added. The solution was washed by aqueous HCl (5%, 100 mL), water (2x100 mL), brine and dried over Na_2SO_4. The solvent was evaporated and the product was purified by column chromatography ($CHCl_3$).

(Z)-4-benzylidene-1-((tert-butyldiphenylsilyl)oxy)-2-methyl-1H-imidazol-5(4H)-one.

Yellowish solid, 1.09 g (83%); mp 135-139°C; 1H NMR (700 MHz, CDCl3) δ 8.02 (d, J = 7.0 Hz, 2H), 7.79 (d, J = 7.9 Hz, 4H), 7.45 (t, J = 7.5 Hz, 2H), 7.41 (t, J = 7.7 Hz, 4H), 7.39-7.33 (m, 3H), 6.96 (s, 1H), 2.06 (s, 3H), 1.27 (s, 9H); 13C NMR (176 MHz, CDCl3) δ 165.0, 160.7, 136.1, 134.9, 133.9, 132.2, 130.7, 130.6, 130.1, 128.6, 127.9, 127.7, 26.9, 19.7, 14.9; HRMS (ESI) m/z: 441.2005 found (calcd. for $C_{27}H_{29}N_2O_2Si$, [M+H]+ 441.1998).

(Z)-1-((tert-butyldiphenylsilyl)oxy)-4-(4-((tert-butyldiphenylsilyl)oxy)benzylidene)-2-methyl-1H-imidazol-5(4H)-one.

Yellow solid, 1.58 g (76%); mp 168-171°C; 1H NMR (700 MHz, CDCl3) δ 7.79 (d, J = 8.8 Hz, 2H), 7.75 (d, J = 7.9 Hz, 4H), 7.70 (d, J = 7.9 Hz, 4H), 7.47-7.42 (m, 4H), 7.40-7.34 (m, 8H), 6.84 (s, 1H), 6.75 (d, J = 8.8 Hz, 2H), 1.99 (s, 3H), 1.23 (s, 9H), 1.10 (s, 9H); 13C NMR (176 MHz, $CDCl_3$) δ 165.0, 159.3, 157.7, 136.2, 135.4, 133.9, 133.1, 132.4, 130.7, 130.6, 130.0, 128.0, 127.9, 127.7, 127.2, 120.1, 26.9, 26.4, 19.7, 19.4, 14.8; HRMS (ESI) m/z: 695.3123 found (calcd. for $C_{43}H_{47}N_2O_3Si_2$, [M+H]+ 695.3125).

4.2.4 Synthesis of (Z)-4-(2-(difluoroboryl)arylidene)-1-hydroxy-2-methyl-1H-imidazol-5(4H)-ones (V and VI)

Corresponding protected imidazolone (1 mmol) was dissolved in dry CH_2Cl_2 (50 mL), molecular sieves 4Å (4 g) and 3Å (4g) were added, followed by a solution of boron tribromide in CH_2Cl_2 (1M, 4 mL) and the reaction mixture was stirred for 120 h at the room temperature. The mixture was filtered; molecular sieves were washed two times by ethanol (20 mL) and once by CH_2Cl_2 (100 mL). The solution was mixed with aqueous HF (20%, 2.5 mL) and stirred for 10 min. The mixture was dissolved with EtOAc (100 mL), washed with potassium carbonate solution (5 %, 2 x50 mL), water (2 x 50 mL) and brine (2 x 50 mL) and dried over Na_2SO_4. The solvent was evaporated and the product was purified by column chromatography ($CHCl_3$/EtOH 10:1)

(Z)-4-(2-(difluoroboryl)benzylidene)-1-hydroxy-2-methyl-1H-imidazol-5(4H)-one V).

Yellow solid, 58 mg (23%); mp ~250°C with decomposition; 1H NMR (700 MHz, DMSO) δ 12.2 (bs, 1H), 7.70 (s, 1H), 7.63 (d, J = 7.7 Hz, 1H), 7.59 (d, J = 7.2 Hz, 1H), 7.46 (t, J = 7.2 Hz, 1H), 7.37 (t, J = 7.5 Hz, 1H), 2.70 (s, 3H); 13C NMR (176 MHz, DMSO) δ 164.5, 159.0, 132.8, 131.7, 131.6, 131.3, 129.4, 127.8, 124.7, 11.4; HRMS (ESI) m/z: 231.0728 found (calcd for $C_{11}H_9BFN_2O_2$, [M-F]+ 231.0741).

(Z)-4-(4-((tert-butyldiphenylsilyl)oxy)-2-(difluoroboryl)benzylidene)-1-hydroxy-2-methyl-1H-imidazol-5(4H)-one (VI).

Orange solid, 126 mg (25%); mp ~200°C with decomposition; 1H NMR (700 MHz, DMSO) δ 8.18 (d, J = 7.0 Hz, 4H), 7.58 (s, 1H), 7.50-7.42 (m, 7H), 7.00 (d, J = 1.5 Hz, 1H), 6.67 (dd, J = 8.3, 1.5 Hz, 1H), 2.62 (s, 3H), 1.05 (s, 9H); 13C NMR (176 MHz, DMSO) δ 162.9, 158.7, 158.6, 134.9, 134.0, 131.7, 130.3, 129.5, 128.1, 126.7, 122.9, 122.4, 118.9, 26.2, 18.9, 11.2; HRMS (ESI) m/z: 485.1865 found (calcd for $C_{27}H_{27}BFN_2O_3Si$, [M-F]+ 485.1868).

4.2.4 Synthesis of (Z)-4-(4-hydroxy-2-(difluoroboryl)benzylidene)-1-hydroxy-2-methyl-1H-imidazol-5(4H)-one (IV)

To the solution of (Z)-4-(4-((tert-butyldiphenylsilyl)oxy)-2-(difluoroboryl)benzylidene)-1-hydroxy-2-methyl-1H-imidazol-5(4H)-one (0.2 mmole) in EtOAc (40 mL) was added tributylammonium fluoride (TBAF) trihydrate (100 mg, 0.32 mmol). The mixture was stirred for 10 min at room temperature, neutralized with 1 mL of acetic acid, washed with water (2x20 mL) and brine (2x20 mL) and dried over Na2SO4. The solvent was evaporated and the product was purified by column chromatography ($CHCl_3$/EtOH 4:1).

Orange solid, 41 mg (78%); mp ~250°C with decomposition; 1H NMR (700 MHz, DMSO) δ 12.0 (bs, 1H), 10.3 (bs, 1H), 7.62 (s, 1H), 7.51 (d, J = 8.4 Hz, 1H), 7.01 (d, J = 1.6 Hz, 1H), 6.75 (dd, J = 8.3, 2.4 Hz, 1H), 2.66 (s, 3H); 13C NMR (176 MHz, DMSO) δ 161.8, 161.6, 158.7, 134.9, 130.6, 124.7, 121.6, 118.5, 115.2, 11.2; HRMS (ESI) m/z: 247.0675 found (calcd for $C_{11}H_9BFN_2O_3$, [M-F]+ 247.0690).

Conclusions

We have described the synthesis of a new pH-dependent fluorescence turn-off switching molecule based on a conformatinally locked green fluorescent protein chromophore. The new switch, *p*OH-BDI-BF_2-*N*OH, is fluorescent only at low pH < 5. The mechanism of operation of the switch is distinct from most other GFP-chromophore-based probes with modulable fluorescence[1]. It operates by a mechanism electronically similar to photochemical *meta*-effects in aryl-containing systems, wherein a electrodonating or mesomeric group placed meta to the conjugated chromophore chain[8-12, 14-15]. We have supported the analogy with the *meta* effect with theoretical calculations. These reveal the intrusion of an orbital into the frontier which cannot couple to the conjugated chromophore, as in the *meta* effect. Excitations out of the uncoupled frontier orbital give rise to a dim excited state of the molecule, which effectively depopulates the fluorophore excited state and quenches the fluorescence. The imidazolinone ring is heteroaromatic and non-alternant, so the identification of sites with *meta*-like photochemical character is not as straightforward as for the aryl ring. In order to identify a candidate site, we leveraged the known frontier electronic structure of the oxonol fluorophore

in BDIs[23-25]. Similar strategies may work in other cases where *meta* effects are desired in non-alternate ring systems.

As the chromophore *p*OH-BDI-BF_2-*N*OH is a fluorophore only at pH < 5, it may prove be useful for imaging cellular structures and organelles with locally low pH, such as lysosomes. Such structures are thought to be important for cellular processes such as endocytosis, phagocytosis, autophagy and apoptosis[49]. In humans the pH of the intracellular compartmens varies from 4.5 (in lysosome lumens) to 7.5-8.0 (in mitochondria matrices). The intercellular pH values vary in a much broader range from 1.0 in stomach liquids to 8.1 in the pancreatic secretion[50-53].

Acknowledgement

The Moscow group acknowledges support from the Russian Foundation for Basic Research Grant 15-03-02856-a. This research was carried out using the equipment provided by IBCH core facility (CKP IBCH). KMS acknowledges generous support from the National Science Foundation (CHE-1213047). SO acknowledges support from Australian Research Council (ARC) Discovery Grants DP110101580 and DP160102425. Computations were performed on the Australian National Computational Infrastructure Facility at ANU using time granted under Merit Allocation Scheme grants m03 and n62.

Notes and references

1. Walker, C. L.; Lukyanov, K. A.; Yampolsky, I. V.; Mishin, A. S.; Bommarius, A. S.; Duraj-Thatte, A. M.; Azizi, B.; Tolbert, L. M.; Solntsev, K. M., *Curr. Opin. Chem. Biol.* **2015,** *27*, 64.
2. Chattoraj, M.; King, B. A.; Bublitz, G. U.; Boxer, S. G., *Proc. Natl. Acad. Sci. USA* **1996,** *93*, 8362.
3. McAnaney, T. B.; Park, E. S.; Hanson, G. T.; Remington, S. J.; Boxer, S. G., *Biochemistry* **2002,** *41*, 15489.
4. McAnaney, T. B.; Shi, X.; Abbyad, P.; Jung, H.; Remington, S. J.; Boxer, S. G., *Biochemistry* **2005,** *44*, 8701.
5. Shi, X.; Abbyad, P.; Shu, X.; Kallio, K.; Kanchanawong, P.; Childs, W.; Remington, S. J.; Boxer, S. G., *Biochemistry* **2007,** *46*, 12014.
6. Dong, J.; Solntsev, K. M.; Tolbert, L. M., *J. Am. Chem. Soc.* **2006,** *128*, 12038.
7. Tolbert, L. M.; Baldridge, A.; Kowalik, J.; Solntsev, K. M., *Acc. Chem. Res.* **2012,** *45*, 171.
8. Solntsev, K. M.; Poizat, O.; Dong, J.; Rehault, J.; Lou, Y.; Burda, C.; Tolbert, L. M., *J. Phys. Chem. B* **2008,** *112*, 2700.
9. Zimmerman, H. E., *J. Phys. Chem. A* **1998,** *102*, 5616.
10. Lewis, F. D.; Kalgutkar, R. S.; Yang, J.-S., *J. Am. Chem. Soc.* **1999,** *121*, 12045.
11. Lewis, F. D.; Kalgutkar, R. S., *J. Phys. Chem. A* **2001,** *105*, 285.
12. Dong, J.; Solntsev, K. M.; Poizat, O.; Tolbert, L. M., *J. Am. Chem. Soc.* **2007,** *129*, 10084.
13. Solntsev, K. M.; McGrier, P. L.; Fahrni, C. J.; Tolbert, L. M.; Bunz, U. H. F., *Org. Lett.* **2008,** *10*, 2429.
14. Yang, J.-S.; Huang, G.-J.; Liu, Y.-H.; Peng, S.-M., *Chem. Comm.* **2008**, 1344.
15. Cheng, C.-W.; Huang, G.-J.; Hsu, H.-Y.; Prabhakar, C.; Lee, Y.-P.; Diau, E. W.-G.; Yang, J.-S., *J. Phys. Chem. B* **2013,** *117*, 2705.
16. Baranov, M. S.; Lukyanov, K. A.; Borissova, A. O.; Shamir, J.; Kosenkov, D.; Slipchenko, L. V.; Tolbert, L. M.; Yampolsky, I. V.; Solntsev, K. M., *J. Am. Chem. Soc.* **2012,** *134*, 6025.
17. Ishida, N.; Moriya, T.; Goya, T.; Murakami, M., *J. Org. Chem.* **2010,** *75*, 8709.
18. Lee, C.-Y.; Chen, Y.-C.; Lin, H.-C.; Jhong, Y.; Chang, C.-W.; Tsai, C.-H.; Kao, C.-L.; Chien, T.-C., *Tetrahedron* **2012,** *68*, 5898.
19. Kamlet, M.; Abboud, J.; Abraham, M.; Taft, R., *J. Org. Chem.* **1983,** *48*, 2877.
20. To quantify the solvent dependence of the fluorescence quantum yield, we performed linear regressions against the Kamlet-Taft solvatochromic parameters for QY and logQY. The results are available in the Supplement, and support the assertions given in the text.
21. Werner, H.-J.; Meyer, W., *J. Chem. Phys.* **1981,** *74*, 5794.
22. Olsen, J., *Int. J. Quantum Chem.* **2011,** *111*, 3267.
23. Olsen, S., *J. Chem. Theory Comput.* **2010,** *6*, 1089.
24. Olsen, S.; McKenzie, R. H., *J. Chem. Phys.* **2011,** *134*, 114520.
25. Olsen, S.; McKenzie, R. H., *J. Chem. Phys.* **2012,** *137*, 164319.
26. Dunning, T. H., *J. Chem. Phys.* **1989,** *90*, 1007.
27. Werner, H.-J.; Knowles, P. J.; Knizia, G., *WIREs Comput. Mol. Sci.* **2012,** *2*, 242.
28. Subotnik, J. E.; Yeganeh, S.; Cave, R. J.; Ratner, M. A., *J. Chem. Phys.* **2008,** *129*, 244101.
29. Azhary, A. E.; Rauhut, G.; Pulay, P.; Werner, H.-J., *J. Chem. Phys.* **1998,** *108*, 5185.
30. Olsen, S., *J. Phys. Chem. B* **2015,** *119*, 2566.
31. Olsen, S.; McKenzie, R. H., *Chem. Phys. Lett.* **2010,** *492*, 150.
32. Olsen, S.; Smith, S. C., *J. Am. Chem. Soc.* **2008,** *130*, 8677.
33. Bravaya, K. B.; Grigorenko, B. L.; Nemukhin, A. V.; Krylov, A. I., *Acc. Chem. Res.* **2011,** *45*, 265.
34. Olsen, S., *J. Phys. Chem. A* **2012,** *116*, 1486.
35. Epifanovsky, E.; Polyakov, I.; Grigorenko, B.; Nemukhin, A.; Krylov, A., *J. Chem. Theory Comput.* **2009,** *5*, 1895.
36. Filippi, C.; Zaccheddu, M.; Buda, F., *J. Chem. Theory Comput.* **2009,** *5*, 2074.
37. Polyakov, I.; Grigorenko, B.; Epifanovsky, E.; Krylov, A.; Nemukhin, A., *J. Chem. Theory Comput.* **2010,** *6*, 2377.
38. Martin, M. E.; Negri, F.; Olivucci, M., *J. Am. Chem. Soc.* **2004,** *126*, 5452.
39. Olsen, S., *J. Chem. Phys.* **2015,** *142*, 044116.
40. Celani, P.; Werner, H.-J., *J. Chem. Phys.* **2000,** *112*, 5546.
41. Azizi, Z.; Roos, B. R. O.; Veryazov, V., *Phys. Chem. Chem. Phys.* **2006,** *8*, 2727.
42. Crompton, E. M.; Lewis, F. D., *Photochem. Photobiol. Sci.* **2004,** *3*, 660.
43. Lewis, F. D.; Crompton, E. M., *J. Am. Chem. Soc.* **2003,** *125*, 4044.
44. Huang, G.-J.; Cheng, C.-W.; Hsu, H.-Y.; Prabhakar, C.; Lee, Y.-P.; Diau, E. W.-G.; Yang, J.-S., *J. Phys. Chem. B* **2013,** *117*, 2695.
45. Hansch, C.; Leo, A.; Taft, R. W., *Chem. Rev.* **1991,** *91*, 165.
46. Rajput, J.; Rahbek, D. B.; Andersen, L. H.; Rocha-Rinza, T.; Christiansen, O.; Bravaya, K. B.; Erokhin, A. V.; Bochenkova, A. V.; Solntsev, K. M.; Dong, J.; Kowalik, J.; Tolbert, L. M.; Petersen, M. Å.; Nielsen, M. B., *Phys. Chem. Chem. Phys.* **2009,** *11*, 9996.
47. Addison, K.; Heisler, I. A.; Conyard, J.; Dixon, T.; Bulman Page, P. C.; Meech, S. R., *Faraday Discuss.* **2013,** *163*, 277.
48. Litvinenko, K.; Webber, N.; Meech, S., *J. Phys. Chem. A* **2003,** *107*, 2616.
49. Turk, B.; Turk, V., *J. Biol. Chem.* **2009,** *284*, 21783.

50. Boron, W. F.; Boulpaep, E. L., *Medical physiology: a cellular and molecular approach*. 2 ed.; Saunders/Elsevier: Philadelphia, PA, USA, 2009.
51. Porcelli, A. M.; Ghelli, A.; Zanna, C.; Pinton, P.; Rizzuto, R.; Rugolo, M., *Biochem. Bioph. Res. Co.* **2005,** *326*, 799.
52. Santo-Domingo, J.; Demaurex, N., *J. Gen. Physiol.* **2012,** *139*, 415.
53. Mindell, J. A., *Annu. Rev. Physiol.* **2012,** *74*, 69-86.